Preliminary Elucidation of the Mechanism Underlying Coal Degradation by *Bacillus amyloliquefaciens*

Chengyong Liu,[a] Weilong Cao,[b] Wenzhe Gu,[a] Zhigang Wang, [c] Yun Zhang,[a] Fengtian Sheng,[a] Beiyan Zhang,[a] Chaofeng Yuan,[a] and Yaya Wang [b,*]

**Corresponding author: wangyaya@xust.edu.cn*

DOI: 10.15376/biores.20.3.7211-7231

GRAPHICAL ABSTRACT

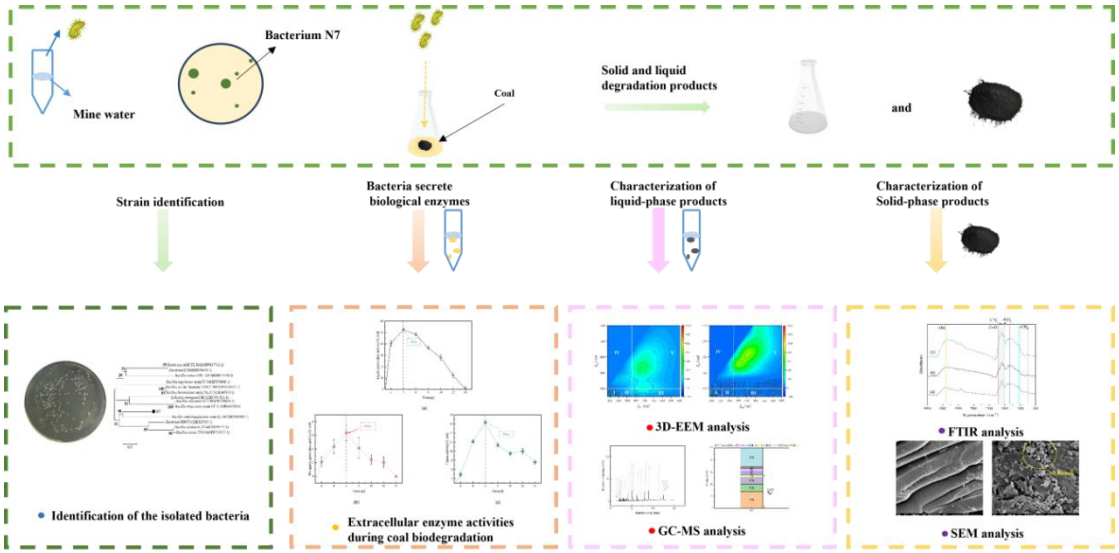

Preliminary Elucidation of the Mechanism Underlying Coal Degradation by *Bacillus amyloliquefaciens*

Chengyong Liu,[a] Weilong Cao,[b] Wenzhe Gu,[a] Zhigang Wang,[c] Yun Zhang,[a] Fengtian Sheng,[a] Beiyan Zhang,[a] Chaofeng Yuan,[a] and Yaya Wang [b,*]

China's abundant low-rank coal faces challenges in utilization due to high moisture content and low calorific value. Microbial biodegradation has emerged as a promising method to improve coal quality. This study investigates the coal-degrading capabilities of the *Bacillus amyloliquefaciens* strain, designated as strain N7 in this study. Experimental results demonstrated that strain N7 significantly degraded lignite. On Luria-Bertani solid medium, the strain formed clear coal solubilization zones, indicating its biodegradation potential. Three-dimensional excitation-emission matrix fluorescence spectroscopy revealed humic-like substances, suggesting humic acid formation through oxidative depolymerization. Enzyme assays identified lignin peroxidase (LiP) and lipase as key contributors, with LiP showing particularly high activity. Scanning electron microscopy showed dense bacterial colonization on coal surfaces, implying efficient biodegradation through direct interaction. Fourier-transform infrared spectroscopy and X-ray photoelectron spectroscopy indicated an increase in free hydroxyl groups in degraded coal, supporting structural breakdown. Degradation products analysis revealed 32% phenolic compounds and 55% long-chain alkanes, providing chemical evidence of lignite decomposition. These results highlight strain N7 as an effective microorganism for lignite biodegradation, offering insights for optimizing microbial coal bioconversion.

DOI: 10.15376/biores.20.3.7211-7231

Keywords: Bacillus amyloliquefaciens; Lignite; Microbial degradation; Enzymes

Contact information: a: China Coal Research Institute Co., Ltd., Xi'an, China; b: College of Chemistry and Chemical Engineering, Xi'an University of Science and Technology, Xi'an, China; c: College of Energy and Mining Engineering, Xi'an University of Science and Technology, Xi'an, China;
** Corresponding author: wangyaya@xust.edu.cn*

INTRODUCTION

In China, the reserves of low-rank coal are abundantly present, mainly distributed in Shanxi, Xinjiang, Inner Mongolia, and Shaanxi (Sivrikaya 2014; Xia *et al.* 2015; Song *et al.* 2016). While these deposits are geographically widespread, their utilization poses significant environmental and operational hurdles. Low-rank coal's inherently high moisture content reduces its combustion efficiency and contributes to elevated emissions of pollutants, including carbon dioxide, sulfur oxides, and nitrogen oxides, exacerbating ecological harm (Xu *et al.* 2017; Zhang *et al.* 2022). In response, microbial biodegradation has gained attention as a sustainable strategy to mitigate these challenges (Akimbekov *et al.* 2022; Rehman *et al.* 2022). This approach employs microorganisms to break down coal-derived organic matter, thereby reducing environment-associated problems while enhancing resource utility (Baylon *et al.* 2017).

Low-rank coal, with its elevated volatile content and porous structure, exhibits high susceptibility to microbial action compared to its higher-rank counterparts (Robbins *et al.* 2016). These intrinsic properties position lignite, a prominent subtype of low-rank coal, as a prime candidate for bioconversion. Consequently, microbial degradation is increasingly recognized as a pivotal pathway for advancing clean coal technologies, offering a dual benefit of pollution reduction and energy optimization (Akimbekov *et al.* 2022).

Recently, significant progress has been made in understanding microbial coal degradation (Achi 1994). Fungal strains, for instance, have demonstrated the ability to solubilize low-rank coal into liquid byproducts, with studies attributing this process to oxidative enzymatic activity (Cohen and Gabriele 1982; Hofrichter and Fritsche 1996; Fakoussa and Hofrichter 1999). For instance, the fungal strain A-1 that was isolated from *Tremella* sp. (white fungus) was applied to Shanxi lignite. Results revealed lignin peroxidase (LiP) as the dominant enzyme in its degradation mechanism. The LiP activity is higher than that of manganese peroxidase, underscoring its critical role in lignite depolymerization (Feng *et al.* 2021). Enzymatic studies by Romanowska *et al*. (2015) further confirmed that peroxidases and hydrolases synergistically destabilize coal macromolecular networks. Laborda *et al*. (1997) isolated the fungal strain M2, which effectively degraded Spanish lignite. Machnikowska *et al.* (2002) demonstrated that nitric acid pretreatment enhances the dissolution efficiency of low-rank coal, with degradation efficacy inversely correlating to coal rank (Machnikowska *et al.* 2002). Despite these advances, bacterial contributions to lignite biodegradation remain underexplored, particularly strains sourced from coal-associated environments such as mine water. Identifying novel bacterial candidates with robust lignite-degrading capabilities could offer valuable insights into scalable biotechnological applications, warranting further systematic investigation.

In this study, a bacterial strain isolated from aqueous environments in the Han Cheng coal mine was systematically evaluated for their lignite degradation potential. Initial screening on Luria-Bertani (LB) solid medium identified strains exhibiting distinct coal solubilization zones, which were subsequently purified and subjected to taxonomic classification *via* 16S rDNA sequencing. To assess biodegradation efficacy, lignite samples treated with the selected strain were analyzed using scanning electron microscopy (SEM) and Fourier-transform infrared spectroscopy (FTIR), X-ray photoelectron spectroscopy (XPS), and X-ray diffraction (XRD), revealing structural and functional group modifications. Liquid-phase degradation products were characterized by gas chromatography-mass spectrometry (GC-MS) and three-dimensional excitation-emission matrix (3D-EEM) fluorescence spectroscopy to identify organic intermediates. This study aimed to elucidate the mechanism underlying microbial lignite degradation.

EXPERIMENTAL

Preparation of Lignite Specimens

Lignite was collected from Datong, Shanxi, and ground to particle sizes ranging from 0.075 to 0.125 mm. A total of 30 g of lignite was mixed with 75 mL of 10 M nitric acid and subjected to oxidation treatment for 48 h under room temperature and ventilated conditions (Wu *et al.* 2022). After oxidation, the samples were thoroughly washed with distilled water until the pH reached or exceeded 6. The washed

lignite was then dried in an oven at 75 °C for 12 h, followed by sterilization in an autoclave at 121 °C for 15 min.

Lignite Characterization

Proximate and ultimate analyses of Shanxi Datong lignite are summarized in Table 1. Proximate analysis showed raw lignite contains 55.03% volatile matter with low fixed carbon. Following nitric acid oxidation, ash content decreased significantly, likely due to dissolution of calcite minerals by acidic treatment. Ultimate analysis demonstrated reduced carbon (C) and hydrogen (H) fractions but elevated nitrogen (N) and oxygen (O) in oxidized lignite. These changes reflect nitric acid's capacity to degrade aromatic networks, generate oxygen-containing groups, and introduce nitro functional groups via electrophilic substitution. Following microbial treatment, C content further decreased, while H and O fractions increased. These transformations align with enzymatic oxidation of aromatic constituents, likely mediated by lignin-modifying peroxidases that destabilize coal macromolecules.

Table 1. Proximate and Ultimate Analyses of Raw, Nitric Acid-Oxidized, and Microbially Degraded Lignite Samples

Coal Samples	Proximate Analysis (wt%)					Ultimate Analysis (wt%)				
	A	V_{daf}	FC_{daf}	M_{ad}		C	H	O	N	S
Raw coal	13.20	55.03	63.38	11.64		73.52	4.86	20.37	0.89	0.18
Oxidized coal	7.71	64.31	51.24	5.48		58.36	4.21	30.62	3.97	0.05
Residual coal	5.84	61.54	44.97	3.46		54.37	4.52	36.86	4.12	0.02

Note: ad, air dry basis; *M*, moisture; *A*, ash; *V*, volatile matter; FC, fixed carbon; ad, air-dried base; daf, dry ash-free basis

Bacterial Isolation and Purification

A mine water sample was collected from the Hanchen coal mine and serially diluted with sterile water from 10^{-1} to 10^{-6}. Then 100 µL of each diluted solution was evenly spread onto agar plates. The agar medium contained 2.5 g of brown coal, 0.5 g of KH_2PO_4, 0.5 g of NH_4Cl, 1.0 g of $MgCl_2$, 0.5 g of NaCl, 0.5 g of yeast extract, 0.2 g of $CaCl_2$, 20 g of agar, 0.1 g of $FeCl_3$, and 1.0 L of sterile water, with a pH adjusted to 7.2. The plates were incubated at 35 °C for 48 h in a biological incubator. After incubation, bacterial colonies were purified using LB solid agar medium.

Identification of Bacterial Strain

Genomic DNA was extracted from the bacterial isolate using a commercial bacterial DNA extraction kit. The 16S rDNA gene was amplified by polymerase chain reaction (PCR) with universal bacterial primers 27F (5′-AGAGTTTGATCC TGGCTCAG-3′) and 1492R (5′-TACCTTGTTACGACTT-3′) (Li *et al.* 2017). The PCR mixture (35 µL total volume) contained 25 µL of 2× Taq PCR Master Mix, 4 µL of template DNA, 2 µL each of forward and reverse primers, and 2 µL of nuclease-free water. Amplification was performed under the following thermocycling conditions: initial denaturation at 95 °C for 5 min; 30 cycles of denaturation at 94 °C for 1.0 min; annealing at 55 °C for 1 min; and extension at 72 °C for 1 min, followed by a final extension at 72 °C for 10 min. Amplicons were purified and sequenced by the Shenggong company (Shanghai, China). The resulting 16S rDNA sequence was aligned

against the NCBI GenBank database using BLAST to determine phylogenetic relationships. A neighbor-joining phylogenetic tree was constructed with MEGA6 software (version 6.0, Koichiro Tamura, Tokyo, Japan) to confirm taxonomic classification.

Coal Solubilization Experiment on Agar Plates

The isolated bacterial strain was streaked onto LB agar plates and incubated at 30 °C for 24 h. Sterilized lignite particles (0.1 g) were then aseptically positioned at the center of each inoculated plate. After seven days of incubation at 30 °C, microbial coal degradation activity was evaluated qualitatively by measuring the diameter of the brown coal solubilization zone surrounding the particles. To quantify biodegradation efficacy, the ratio of the solubilization zone diameter to the bacterial colony diameter was calculated, as previously described (Romanowska *et al.* 2015).

Determination of Extent of Degradation

The coal biodegradation efficiency was quantified using the extent of degradation (η) (Yao *et al*. 2012), defined as,

$$\eta=\frac{\text{M-m}}{\text{M}}\times 100\% \quad (1)$$

where η represents the degradation rate, M is the initial weight of the coal sample (g), and m is the weight of the residual coal sample (g) after biodegradation.

Biodegradation Experiment of Coal

Sterilized lignite was combined with 90 mL of sterile liquid culture medium in 250-mL Erlenmeyer flasks. Subsequently, 10 mL of an overnight bacterial culture was added to each flask. The flasks were incubated at 30 °C at a speed of 160 rpm for 14 days. Control experiments were prepared by replacing the bacterial inoculum with an equivalent volume of sterile saline solution. All treatments were performed in triplicate. Following incubation, the solid and liquid phases were separated *via* centrifugation at 10,000 × g for 20 min. The residual coal fraction was oven-dried at 75 °C for 48 h, while the supernatant was filtered through a 0.22-μm membrane and stored at −80 °C for subsequent analysis.

Measurement of A_{450}

During biodegradation, 3 mL aliquots of culture broth were aseptically collected every 48 hours. Samples were centrifuged at 10,000 × *g* for 10 minutes to remove suspended solids. The supernatant was diluted 50-fold with distilled water, and absorbance at 450 nm was measured using a UV-Vis spectrophotometer (TU-1950, Purkinje General Instrument, Beijing, China).

Enzyme Activity Assays

Lignin peroxidase activity assay

LiP enzyme activity was determined using a modified protocol based on Rath *et al*. (2022). The reaction mixture consisted of 0.1 mL of 1.2 mmol/L methylene blue (MB), 0.6 mL of 0.5 mol/L sodium tartrate buffer (pH 4.0), and 2 mL of the supernatant sample. The reaction was initiated by adding 0.1 mL of 2.7 mmol/L hydrogen peroxide (H_2O_2), followed by immediate vortex. At specified intervals, 1 mL of reaction mixture was diluted tenfold with deionized water, and then analyzed at 664 nm using a

spectrophotometer. Absorbance was recorded at 1.0- and 6.0-min post-initiation, the enzyme activity (U/mL) was calculated using formula (2),

$$U=\frac{(A_1-A_6)\times 2800}{\varepsilon MB} \quad (2)$$

where U represents the enzyme activity (U/mL), A_1 is the absorbance at 1.0 minute, A_6 is the absorbance at 6.0 minutes, and εMB is the molar extinction coefficient of methylene blue at 664 nm ($L\cdot mol^{-1}\cdot cm^{-1}$). The value 2800 is a composite constant ($mL\cdot L\cdot \mu mol^{-1}\cdot min$).

Determination of manganese peroxidase activity

The reaction mixture was comprised of 1.0 mL of 50 mM guaiacol, 0.6 mL of 100 mM sodium tartrate buffer (pH 4.5), and 2 mL of supernatant. The reaction was initiated by adding 0.1 mL each of 0.1 mM H_2O_2 and 1 mM $MnSO_4$, followed by thorough vortexing. After incubating at room temperature for 3 min, absorbance at 469 nm was measured at 1- and 6-min post-initiation to monitor the formation of oxidized guaiacol derivatives. Enzyme activity (U/mL) was calculated using the formula (3) described previously (Dahdouh *et al.* 2020).

$$U=\frac{(A_6-A_1)\times 148}{\varepsilon} \quad (3)$$

where U denotes enzyme activity in units per milliliter (U/mL), A_1 and A_6 are the absorbance values at 1.0 and 6.0 minutes, respectively, and ε is the molar extinction coefficient of the oxidized guaiacol derivative at 469 nm ($L\cdot mol^{-1}\cdot cm^{-1}$). The value 148 is a composite constant ($mL\cdot \mu mol^{-1}$).

Determination of lipase activity

To measure the lipase activity, 2 mL of the substrate solution (composed of a 4% polyvinyl alcohol and olive oil mixture in a 3:1 volume ratio) was combined with 5 mL of phosphate buffer solution (pH 7.5). After adding 1.0 mL of the supernatant sample, the mixture was incubated in a water bath at 40 °C for 15 min. Following incubation, the mixture was allowed to stand at room temperature for 5 min. Subsequently, 8 mL of a 95% ethanol solution and 25 µL of phenolphthalein indicator were added. The solution was then titrated with 0.05 mol/L NaOH until a stable red color persisted for at least 30 s, indicating the endpoint of the titration. Enzyme activity was calculated using the formula (4) provided in the literature (Indriyani *et al.* 2021).

$$U=\frac{(v_s-v_b)\times c_N}{t\times v_e}\times 6000 \quad (4)$$

where U represents the enzyme activity (U/mL), V_s is the volume of NaOH consumed at the titration endpoint (mL), V_b is the volume of NaOH consumed in the blank control (mL), C_N is the concentration of NaOH titrant (mol/L), t is the reaction time (min), and V_e is the volume of the sample added (mL). The value 6000 is a composite constant ($mL\cdot L\cdot \mu mol^{-1}\cdot min$).

Characterization of Degradation Products

FTIR spectroscopy

Approximately 1.0 mg of the lignite sample and 100 mg of potassium bromide were weighed and dried in a constant-temperature oven at 85 °C for 3 h. After drying, the lignite sample and potassium bromide were transferred into a quartz mortar and

mixed thoroughly. The mixture was ground until a uniform gray powder was obtained and then compressed it into a thin sheet using a hydraulic press to complete the sample preparation. Finally, the sample was scanned in the wavelength range of 4000 to 400 cm^{-1} with a resolution of 4 cm^{-1} using an infrared spectrometer (Nicolet iN10-iZ10, Thermo Fisher Scientific, Waltham, MA, USA).

XPS analysis

Lignite samples (raw, nitric acid-oxidized, and degraded residual; 50 mg each) were analyzed using a Thermo Scientific K-Alpha spectrometer (Thermo Fisher Scientific, MA, USA). Measurements employed Al Kα radiation (1486.6 eV) with a 400 µm beam spot, 12 kV accelerating voltage, 6 mA filament current, and 60° electron emission angle. The full-spectrum scan covered an energy range of 150 eV with a step size of 1 eV, while the narrow-spectrum scan covered 50 eV with a step size of 0.1 eV. The narrow-spectrum scan was conducted with at least five signal accumulation cycles.

XRD analysis

Dried lignite samples (30 mg each) were characterized *via* a Bruker D8 Advance diffractometer (Bruker Corporation, Karlsruhe, Germany). XRD scanning was performed at a scanning rate of 10°/min within the 5° to 90° testing angle range.

SEM analysis

The lignite sample was placed in a constant-temperature oven set to 85 °C and dried for 3 h. Next, 50 mg of the dried coal sample was accurately weighed and analyzed using a ZEISS Sigma 300 scanning electron microscope (Carl Zeiss AG, Germany) with a resolution of 1.06 nm.

GC-MS analysis

The liquid phase sample was filtered through a 0.22-µm membrane. Subsequently, 1.0 mL of the filtrate was mixed with 2 mL of dichloromethane and extracted for 3 to 4 h. Following extraction, 1.0 mL of the sample was collected for analysis. The GC-MS (Agilent 8890-5977B; Agilent, Palo Alto, CA, USA) was performed using an HP-5ms column (30 m × 250 µm × 0.25 µm) with a constant flow rate of 1 mL/min. The temperature program began at 60 °C (held for 1 min), increased to 150 °C at 10 °C/min, and then ramped to 310 °C at 4 °C/min (held for 10 min).

3D-EEM fluorescence measurement

The supernatant samples were analyzed using a 3D-EEM fluorescence spectroscopy (Duetta; HORIBA Instruments Incorporated, Kyoto, Japan) under the following conditions: an excitation range of 225 nm to 450 nm, with a step size of 5 nm, and an emission range from 270 nm to 600 nm. Both the excitation and emission bandwidths were set to 5 nm. The integration time for each scan was 0.1 s, and the resulting spectral data were recorded and plotted for analysis.

RESULTS

Coal Biodegradation by the Isolated Bacteria

Several bacterial strains were isolated from mining water samples. Among the isolates, strain N7 exhibited the highest lignite degradation efficiency, as determined by comparative analysis of coal solubilization zones on LB agar plates. Thus, strain N7

was selected for further investigation into the microbial degradation mechanisms of coal.

As shown in Fig. 1, a dark brown dissolution halo with a diameter of 4.9 cm formed around the sterile brown coal particles after 7 days of incubation, indicating the degradation of lignite. Concurrently, the medium transitioned from pale yellow to brown, with visible reduction in coal particles. These morphological changes demonstrate strain N7's capacity to degrade lignite. The degradation rate, calculated using the weighing method, was found to be 20.8%.

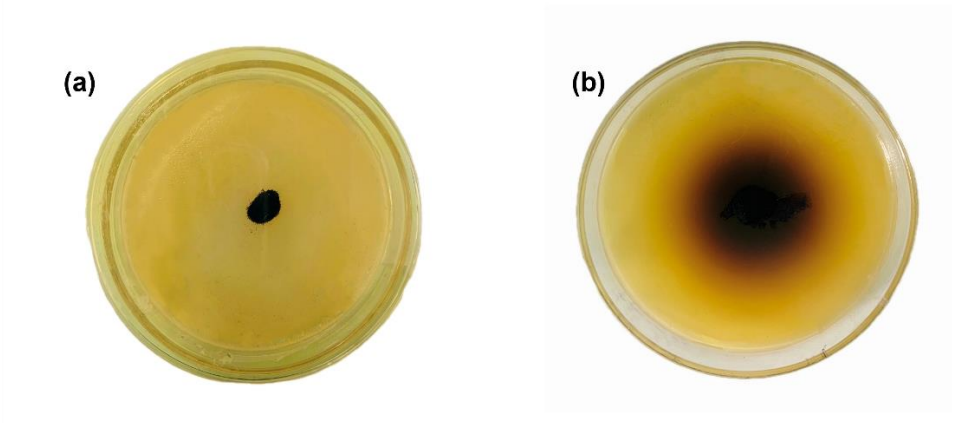

Fig. 1. Degradation of lignite particles on LB agar plates (a) before and (b) after strain N7 addition

The Analysis of A_{450} During Coal Biodegradation

The absorbance value at 450 nm (A_{450}) was reported to be a reliable and efficient measure for assessing the degree of coal degradation (Shi *et al.* 2009).

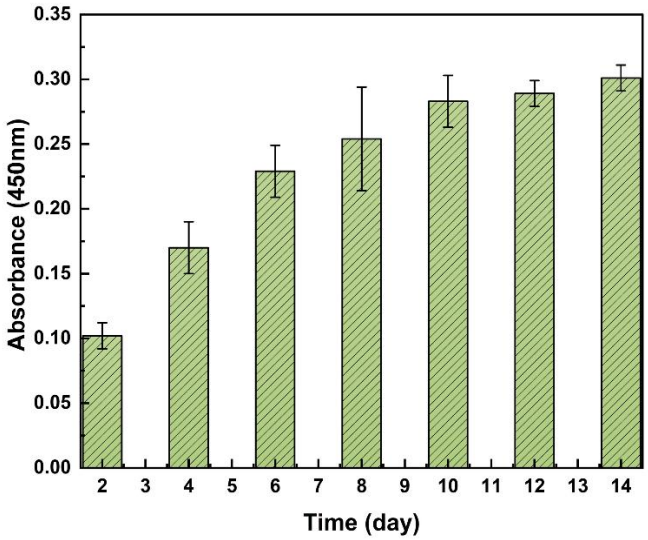

Fig. 2. Absorbance at 450 nm (A_{450}) during the lignite biodegradation process

As illustrated in Fig. 2, during lignite biodegradation, the A_{450} values of the degradation solution steadily increased during the first 10 days, accompanied by a progressive darkening of the solution. On the 10th day, the A_{450} value plateaued, indicating that the degradation process had nearly reached completion.

Analysis of 3D-EEM Fluorescence Spectra

The 3D-EEM fluorescence spectra of the control and bacteria-treated supernatant samples are shown in Fig. 3. The spectra were categorized into five distinct regions based on excitation (Ex: 200 to 420 nm) and emission (Em: 240 to 600 nm) wavelength ranges, each corresponding to specific dissolved organic matter (DOM) components. Region I (Ex: 200 to 250 nm; Em: 240 to 330 nm) is indicative of tyrosine-like substances, while Region II (Ex: 200 to 250 nm; Em: 330 to 380 nm) corresponds to tryptophan-like substances. Region III (Ex: 200 to 330 nm; Em: 380 to 600 nm) represents humic acid-like compounds, and Region IV (Ex: 250 to 420 nm; Em: 240 to 380 nm) aligns with soluble microbial byproducts. Region V (Ex: 250 to 420 nm; Em: 380 to 600 nm) is characteristic of humic substance-like materials (Zhou *et al.* 2013).

Figures 3a and 3b present the 3D-EEM fluorescence spectra of the control group (without bacteria addition) and the degradation solution from strain N7 treated group, respectively. Both spectra exhibit high fluorescence intensity in Region V. Notably, the fluorescence intensity in the degradation solution from strain N7 treatment is higher than that of the control group. This increase is likely due to the production of humic acid (HA) during the lignite biodegradation process. The accumulation of HA is a key indicator of biological dissolution (Nsa *et al.* 2022). Fakoussa *et al*. (1999) have shown that the concentration of HA correlates with the magnitude of the A_{450} value, a higher A_{450} value reflects a greater concentration of HA. These results suggest that strain N7 effectively promotes lignite degradation.

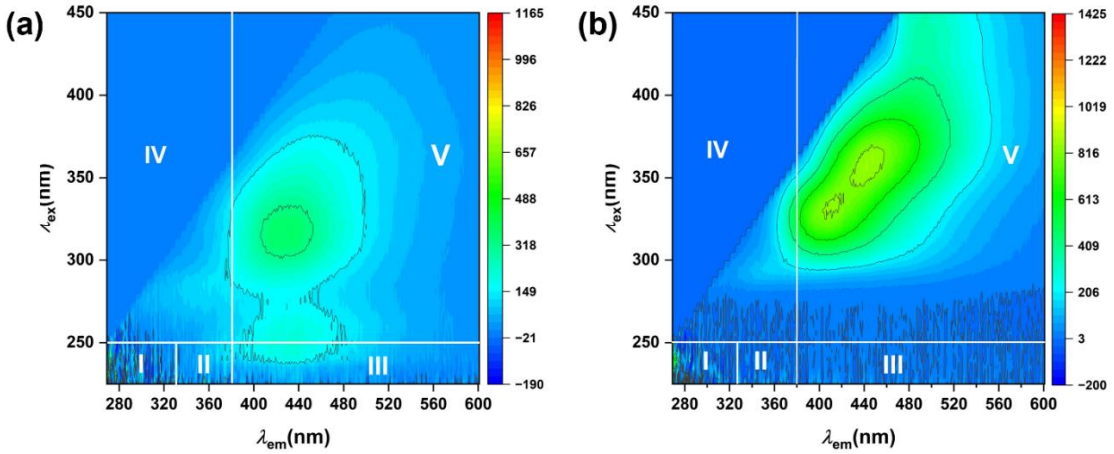

Fig. 3. 3D-EEM fluorescence spectra of the supernatant obtained from (a) control and (b) bacterial-treated samples

Identification of the Isolated Bacteria

Figure 4 displays the morphological characteristics and DNA sequence-based phylogenetic tree of the bacterial strain N7.

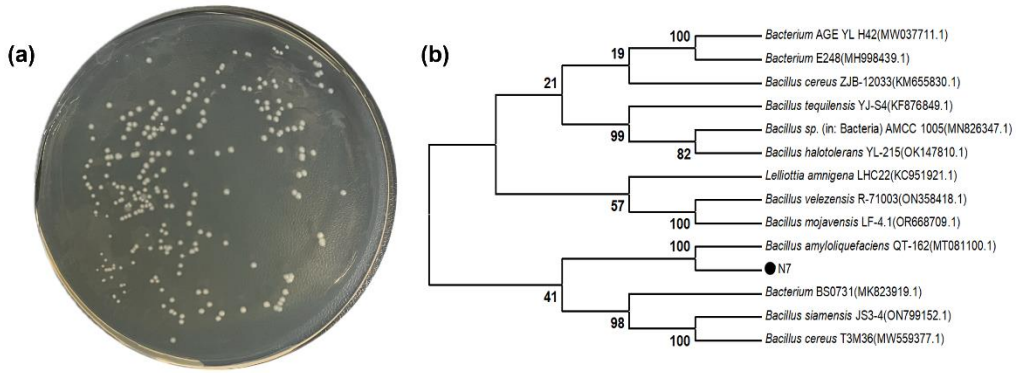

Fig. 4. (a) The colony morphology, and (b) phylogenetic tree of the N7 bacterial strain

As shown in Fig. 4a, the N7 strain exhibited a round shape with an off-white coloration, a slightly elevated white center, and smooth edges. Figure 4b demonstrates that the 16S rDNA gene sequence of N7 closely aligns with that of *Bacillus amyloliquefaciens*, a species within the *Bacillus* genus.

Extracellular Enzyme Activities During Coal Biodegradation

The activities of lignin peroxidase, manganese peroxidase, and lipase were measured over the course of the lignite biodegradation experiment.

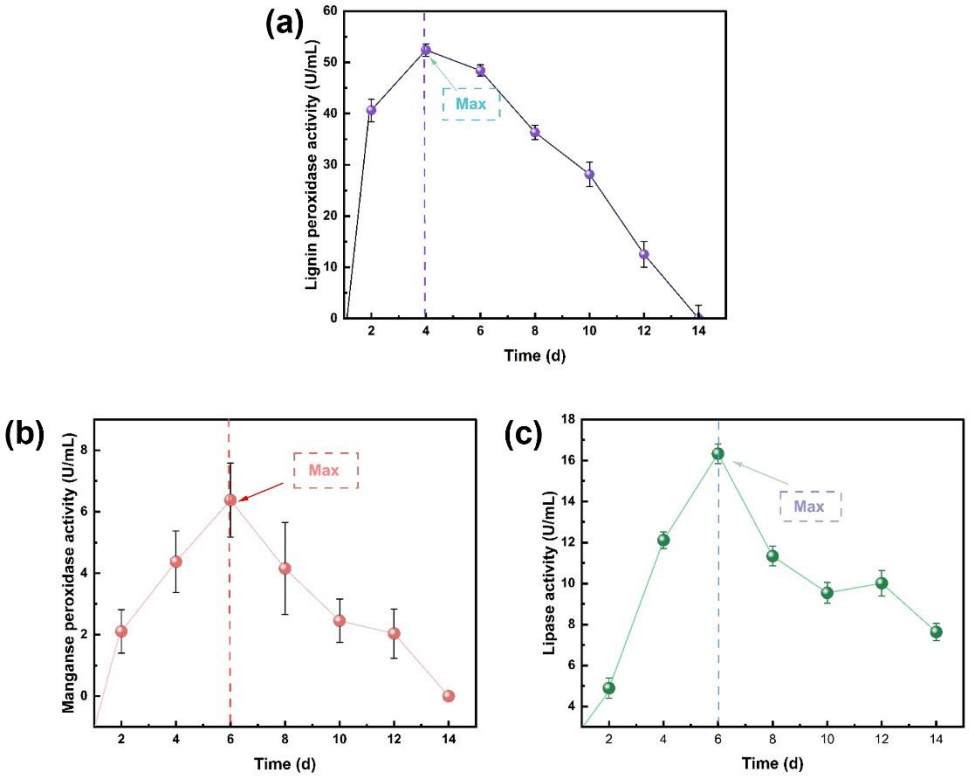

Fig. 5. Enzymatic activities of (a) lignin peroxidase, (b) manganese peroxidase, and (c) lipase during the lignite biodegradation process

The LiP activity peaked on day 4 (52.40 U/mL) before declining to negligible levels by day 14, while MnP and lipase activities increased steadily, reaching maxima on day 6 (6.37 U/mL and 16.33 U/mL, respectively) (Fig. 5). Notably, LiP activity rose sharply from 40.64 U/mL on day 2 to 52.40 U/mL on day 4, and MnP activity increased from 2.10 U/mL to 6.37 U/mL over the same period, underscoring their critical roles in

the early degradation stage (days 4 to 6). Lipase activity also correlated strongly with early-stage degradation, rising from 4.89 U/mL on day 2 to 16.33 U/mL by day 6.

These enzymes target key structural components of lignite. For instance, LiP facilitates coal degradation by cleaving aromatic rings and oxidizing complex organic polymers (Ralph and Catcheside 1994; Shi *et al.* 2023), whereas MnP oxidizes polycyclic aromatic hydrocarbons (PAHs) (Huang *et al.* 2013). Lipase likely promotes lignite solubilization by hydrolyzing ester bonds in coal-derived organic matter, further destabilizing its macromolecular structure. Collectively, these enzymatic activities highlight strain N7's ability to synergistically degrade lignite through complementary biochemical mechanisms.

Characterization of Liquid Products during Coal Biodegradation

The GC-MS analysis revealed that 16 compounds were detected from the dichloromethane-extracted supernatant samples, including alcohols, acids, esters, phenols, and alkanes with molecular weights ranging from 142 to 441 (Fig. 6a). The presence of long-chain alkanes (> C12) and simplified aromatic derivatives (*e.g.*, phenols, esters) indicates cleavage of coal macromolecules by strain N7 (Shi *et al.* 2024). The extracted retention times, molecular structures, and contents are shown in Table 2.

Table 2. Composition of Main Compounds in Liquid Phase Products

Retention Time (min)	Material Structure	Material Content (%)
5.693	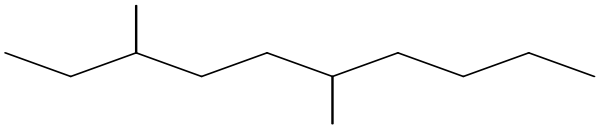	2.46
8.811	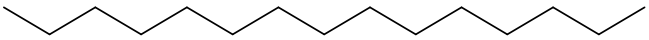	2.49
9.428	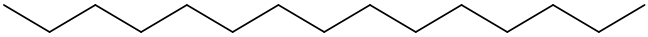	3.81
11.828		1.71
12.546	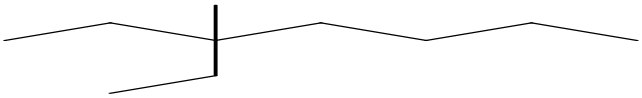	1.56
15.653	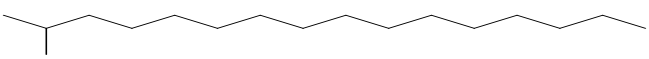	1.54
16.517	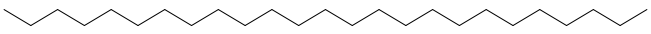	1.52
20.106	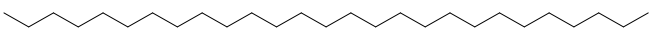	3.75
20.857	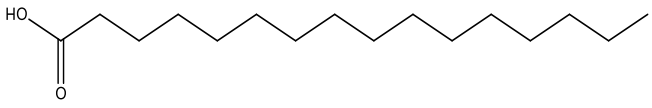	2.46

Retention Time (min)	Material Structure	Material Content (%)
21.003		2.40
24.649		1.40
25.535		2.51
29.023		1.53
32.063	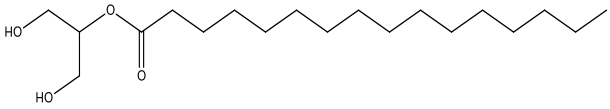	1.68
35.876	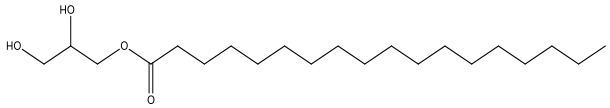	1.85
47.385	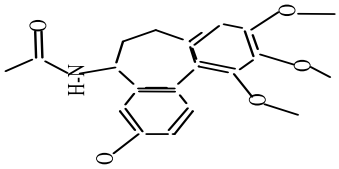	69.01

The composition and proportion of organic matter in the liquid-phase after degradation by strain N7 are presented in Fig. 6b. Alkanes were found to constitute 55% of the degradation products, with short-chain alkanes (< C16) predominating (27%). Long-chain alkanes (> C25) accounted for 4%, while C16 to C20 and C21 to C25 alkanes each represented 12%. Phenolic compounds (32%), alcohols (6%), esters (5%), and acids (2%) comprised the remaining organic fractions. The high alkane yield underscores strain N7's capacity to depolymerize lignite into aliphatic hydrocarbons, further validating strain N7's robust lignite-degrading capability (Schmid and Verger 1998; Barth *et al.* 2004; Yang and Feng 2022).

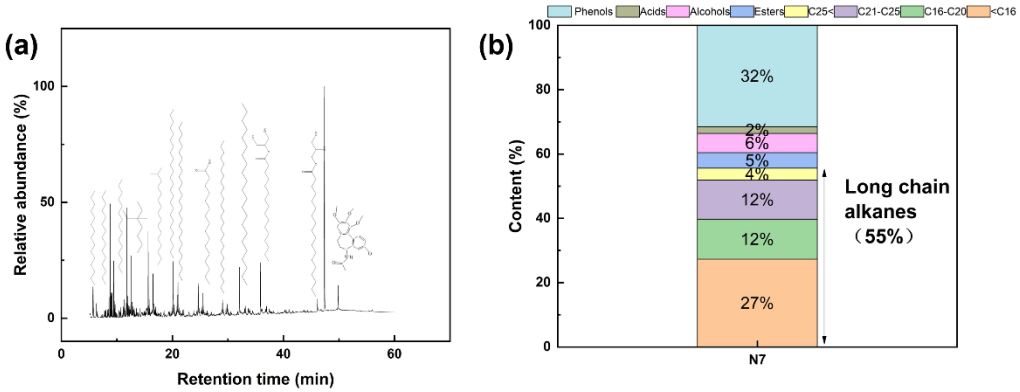

Fig. 6. (a) GC-MS chromatogram of dichloromethane-extracted liquid products degraded by strain N7 and (b) relative contents of organic substances obtained from supernatant samples after N7 degradation

Modifications of Coal after Bacterial Treatment

The FTIR spectra of raw coal, nitric acid-oxidized coal, and strain N7-degraded residual coal are presented in Fig. 7.

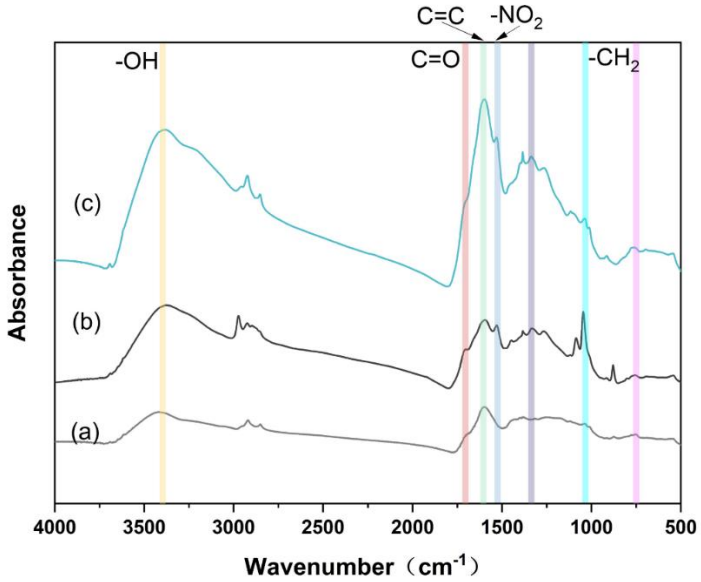

Fig. 7. FTIR spectra of (a) raw coal, (b) oxidized coal, and (c) N7-treated oxidized coal

While the overall spectral profiles of the three samples were similar, significant differences emerged in specific wavenumber regions, reflecting structural modifications induced by microbial degradation. A broad absorption band between 3600 and 3200 cm^{-1}, attributed to hydroxyl (-OH) stretching vibrations (Schmid and Verger 1998), was markedly intensified in the residual coal compared to raw and oxidized coal. This suggests that strain N7 enhanced the formation of free -OH groups, potentially facilitating lignite depolymerization. At 1700 cm^{-1}, the carbonyl (C=O) absorption peak present in raw and oxidized coal disappeared in the residual coal, likely due to lipase-mediated hydrolysis of ester bonds by strain N7. Notably, new absorption peaks at 1530 cm^{-1} and 1338 cm^{-1} emerged in both oxidized and residual coal but were absent in raw coal. The 1530 cm^{-1} peak corresponds to nitro (N=O) groups formed during nitric acid pretreatment (Elbeyli *et al.* 2006), while the 1338 cm^{-1} peak reflects aromatic rings and alkyl side chains (Shi *et al.* 2024). These changes confirm that nitric acid oxidation alters coal's native structure, while microbial activity further modifies its chemical composition.

XPS analysis was conducted to compare the carbon (C) and oxygen (O) contents of raw coal, oxidized coal, and degraded residual coal. The results, shown in Fig. 8, reveal that the C1s content of raw coal, oxidized coal, and degraded residual coal were 93.86%, 83.92%, and 80.37%, respectively, while the O1s content was 5.74%, 16.33%, and 14.57%, respectively. These findings indicate a significant decrease in C content and a corresponding increase in O content after oxidation. Following microbial degradation by strain N7, the C content continued to decrease, while the O content increased. The peak fitting results for the C1s and O1s spectra, shown in Fig. 9, identified the binding energies of C1s as 284.8, 286.6, and 289.0 eV, corresponding to C-C/C-H (carbon-hydrogen and carbon-carbon bonds), -C-O-C/-C-O-H (alcohol, phenol, or ether structures), and C=O (carbonyl or α, β-unsaturated carbonyl) groups (Xia and Zhang 2017). For O1s, the binding energies of 532.5±0.5 eV and 534.0±0.5 eV corresponded to C–O bonds and COO groups, respectively (Pietrzak *et al.* 2007).

The peak fitting data in Tables 3 and 4 show that oxidation resulted in a reduction of -C-C-/-C-H bonds in raw coal from 70.57% to 55.23%. Concurrently, -C-O-C/-C-O-H bonds and -C=O bonds increased from 10.51% and 4.36% to 12.96% and 7.96%, respectively. This suggests that oxidation caused the breakdown of -C-C-/-C-H bonds, leading to the formation of oxygen-containing functional groups such as -C-O-C/-C-O-H and -C=O.

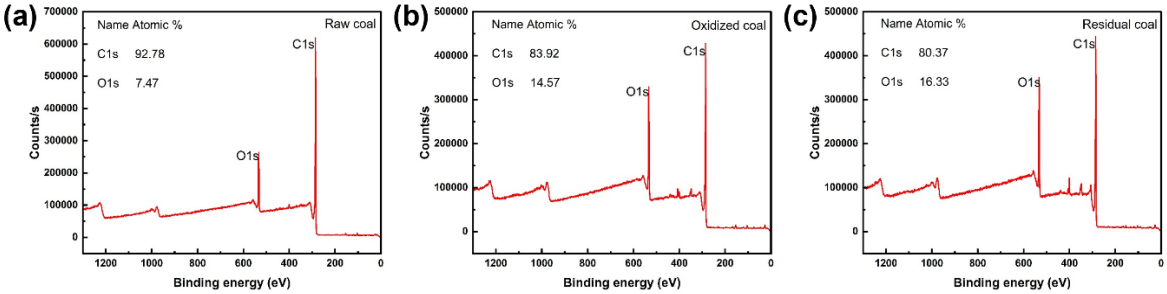

Fig. 8. X-ray Photoelectron Spectroscopy of lignite samples: (a) Raw coal, (b) Nitric acid-oxidized coal, (c) Strain N7-degraded coal

Following bacterial degradation of oxidized coal, the -C-C-/-C-H bonds decreased further from 55.23% to 25.67%, while the -C-O-C/-C-O-H bonds and -C=O bonds increased from 12.96% and 7.96% to 38.48% and 9.43%, respectively. These changes are likely due to the enzymatic activities of lignin peroxidase and manganese peroxidase secreted by strain N7. Lignin peroxidase targets C-C bonds, breaking down macromolecular compounds in coal, while manganese peroxidase acts on C-H bonds.

Table 3. Speciation Analysis of XPS Carbon Spectra Before and After Bacterial Degradation

Coal	Name	Peak BE	Area (P) CPS.eV	Atomic (%)
Raw coal	-C-C-/-C-H	284.80	208548.06	70.57
	-C-O-C/-C-O-H	286.63	31024.14	10.51
	-C=O	288.62	12866.15	4.36
Oxidized coal	-C-C-/-C-H	284.80	142790.35	55.23
	-C-O-C/-C-O-H	286.31	33487.07	12.96
	-C=O	288.96	20534.89	7.96
N7 residual coal	-C-C-/-C-H	284.80	61493.41	25.67
	-C-O-C/-C-O-H	286.64	92153.39	38.48
	-C=O	288.46	22531.61	9.43

The enzymatic activity assays conducted in this study confirmed the presence of lignin peroxidase, manganese peroxidase, and lipase. Moreover, after oxidation, the content of -C-O and -COO bonds increased from 3.88% and 4.62% to 7.89% and 11.69%, respectively. Following bacterial degradation by strain N7, -C-O content rose to 10.44%, while -COO content decreased to 6.44%, likely due to the action of lipase on ester bonds.

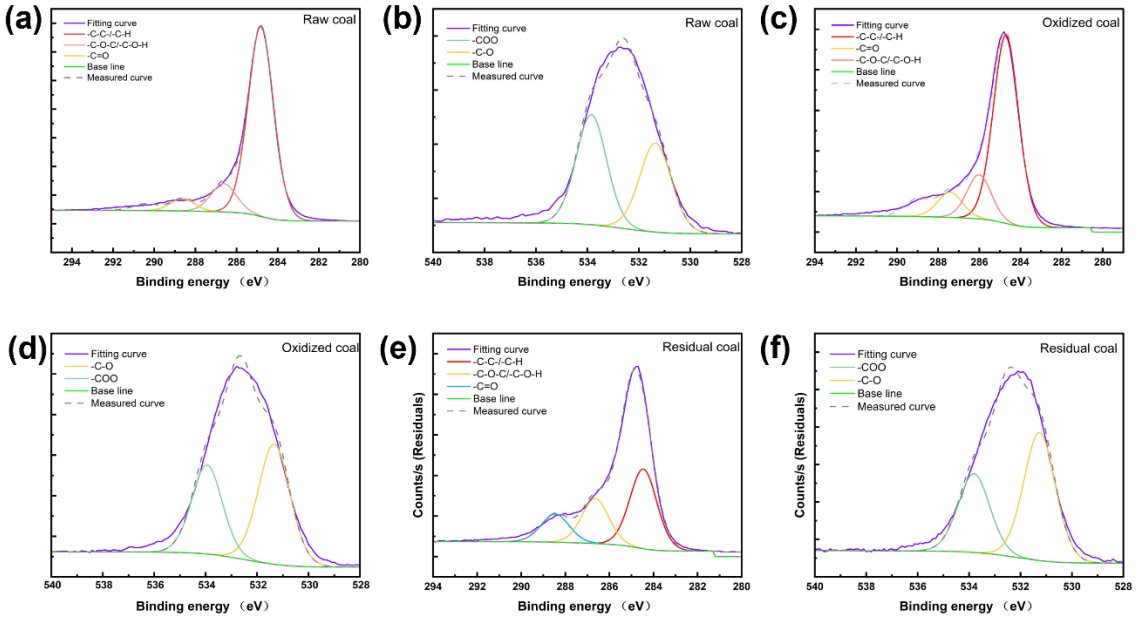

Fig. 9. XPS peak fitting of carbon and oxygen spectra in different lignite samples. (a and b) C1s and O1s deconvolution of raw coal; (c–d) C1s and O1s deconvolution of nitric acid-oxidized coal; (e–f) C1s and O1s deconvolution of microbial-degraded coal

Table 4. Speciation Analysis of XPS Oxygen Spectra Before and After Bacterial Degradation

Coal	Name	Peak BE	Area (P) CPS.eV	Atomic (%)
Raw coal	-C-O	531.95	25901.88	3.88
	-COO	533.84	30787.05	4.62
Oxidized coal	-C-O	531.93	46676.81	7.89
	-COO	533.68	69121.10	11.69
N7 residual coal	-C-O	531.86	53521.50	10.44
	-COO	533.81	32927.29	6.44

XRD analysis of raw coal, nitric acid-oxidized coal, and microbial-degraded lignite revealed distinct mineralogical evolution (Fig. 10). All samples contained graphite, quartz, and hematite as primary mineral phases. A distinct peak at $2\theta = 29.4°$, corresponding to the calcite ($CaCO_3$), was observed in the raw coal, indicating the presence of calcite. Following nitric acid oxidation, this peak disappeared, reflecting the dissolution of calcite in nitric acid and the subsequent reduction of inorganic components in the lignite, which facilitates subsequent microbial degradation by increasing the accessibility of the coal matrix.

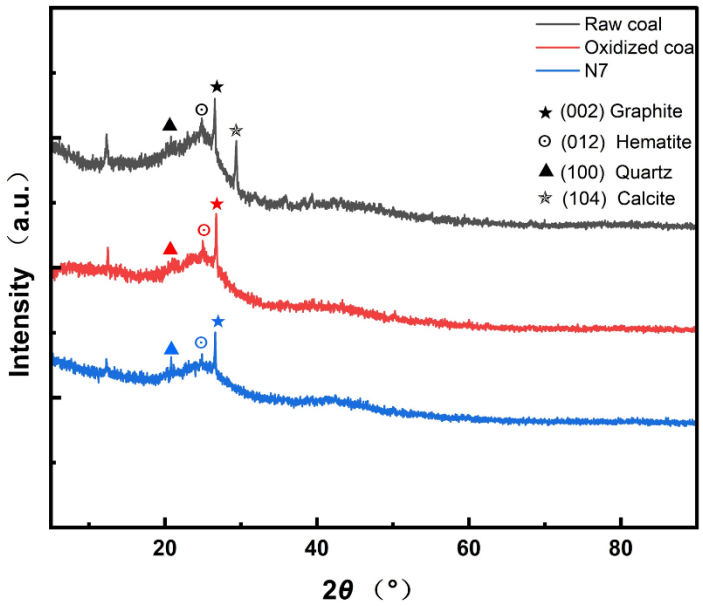

Fig. 10. XRD spectra of various lignite samples

The graphite reflection at $2\theta = 26°$ appeared in all samples, indicating persistent aromatic layering (Bin *et al.* 2024). However, this peak broadened significantly in bacterial-degraded lignite, contrasting with sharper profiles in raw and oxidized samples. Peak broadening inversely correlates with aromatic stacking order (Qingzhao *et al.* 2018). This broadening indicates a reduction in the aromaticity of the coal structure, consistent with the enzymatic activities of lignin peroxidase and manganese peroxidase produced by strain N7, which target and cleave aromatic compounds within the coal matrix.

Absorption of Microbacteria on Coal Surface

The SEM images of untreated lignite samples and those degraded by strain N7 are presented in Fig. 11.

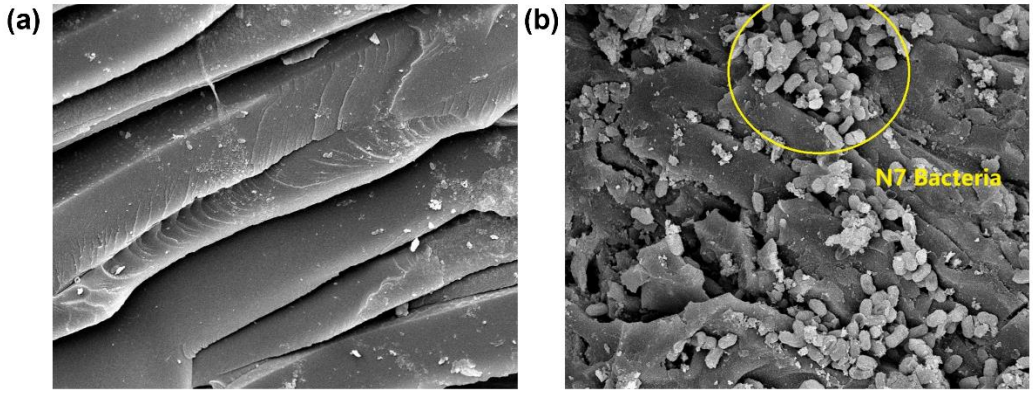

Fig. 11. SEM images of (a) untreated and (b) bacterial-treated lignite

As shown, strain N7 was able to adsorb onto the surface of lignite. A higher adsorption rate of bacteria on the lignite surface increases the likelihood of effective interaction between the bacteria and lignite, thereby enhancing the degradation

efficiency (Guo *et al.* 2018). The images clearly reveal that the surface of untreated lignite was smooth and regular, while the lignite degraded by strain N7 exhibited a rough, loose texture with numerous irregular protrusions and cracks. These surface alterations likely result from bacterial activity, which may induce structural changes in the lignite during degradation, thereby promoting further microbial adsorption.

DISCUSSION

This study isolated several bacterial strains from mine water, identifying *Bacillus amyloliquefaciens* strain N7 as a robust degrader of Shanxi lignite through 16S rDNA sequencing. Strain N7 demonstrated obvious lignite solubilization on LB agar plates, evidenced by pronounced dissolution zones around coal particles. Time-dependent A_{450} measurements revealed a steady increase in solubilized organics from day 0 to day 10, plateauing by day 14. The 3D-EEM fluorescence spectroscopy further corroborated these findings, with degradation products exhibiting elevated fluorescence intensity in the humic-like region (Region V), consistent with enhanced humification (Galib *et al.* 2021). These results validate EEM as a reliable tool for assessing coal biodegradation, complementing traditional A_{450} metrics (Xiao *et al.* 2009). Notably, to the best of the authors' knowledge, this study is the first to report *Bacillus amyloliquefaciens*-mediated lignite biodegradation.

Strain N7 demonstrated the capability to produce extracellular LiP, MnP, and lipase, which aligns with previous reports of *Bacillus amyloliquefaciens*' biocatalytic versatility (Mei *et al.* 2020). For instance, Khan *et al*. (2020) found that *Bacillus amyloliquefaciens* can produce highly active and stable lipases, which is consistent with the findings in this study. The GC-MS analysis revealed phenolic compounds, long-chain alkanes (> C25), and esters in degradation products, implicating the biodegradation of lignite by strain N7 probably through the activities of the extracellular enzymes (Rasiya and Denoj 2021). The SEM imaging confirmed bacterial adhesion to coal surfaces, likely facilitated by extracellular polymeric substances (EPS) that enhance microbe-substrate interaction, a phenomenon also observed by Malik *et al*. (2016) and Shi *et al*. (2024). The FTIR spectroscopy revealed increased hydroxyl (-OH) groups in residual coal, consistent with oxidative cleavage of aromatic networks, while nitric acid pretreatment introduced nitro (N=O) groups and alkyl-aromatic moieties that enhanced structural accessibility (Yin *et al.* 2009). XPS confirmed the enzymatic conversion of aliphatic carbon groups (C–C/C–H) to oxygenated functionalities (C–O, C=O), facilitating macromolecular destabilization. Concurrently, XRD results further showed a reduction in coal aromaticity following microbial treatment. Collectively, these findings support the ability of strain N7 to degrade coal through oxidative and structural modifications.

Despite these advances, challenges persist. Nitric acid pretreatment, though effective, poses environmental risks, necessitating greener alternatives. The mechanistic role of EPS in bacterial adhesion and the precise interplay of LiP, MnP, and lipase during lignite depolymerization warrant deeper exploration. Nevertheless, this work establishes strain N7 as a promising candidate for lignite biodegradation, offering insights into enzymatic synergies and degradation byproducts.

CONCLUSIONS

This study identified *Bacillus amyloliquefaciens* strain N7, isolated from mine water, as a novel microbial agent capable of degrading lignite from Datong, Shanxi.

1. The comprehensive characterization of degradation products and enzymatic activity preliminarily elucidated the key mechanisms underlying strain N7's lignite biodegradation.
2. The scanning electron microscopy (SEM) analysis confirmed bacterial adhesion to coal surfaces, likely mediated by extracellular polymers, which enhanced microbial contact and degradation efficiency.
3. Furthermore, enzymatic activity assays highlighted lignin peroxidase (LiP) as the dominant biocatalyst, with manganese peroxidase (MnP) and lipase contributing synergistically to lignite depolymerization.
4. The gas chromatography – mass spectrometry (GC-MS) analysis detected phenolic compounds (32%) and long-chain alkanes (55%) as dominant degradation byproducts.

This study established *Bacillus amyloliquefaciens* strain N7 as a promising candidate for lignite biodegradation. The findings advance the understanding of microbial coal degradation mechanisms, particularly the roles of LiP, lipase, and MnP, and bacterial adhesion dynamics.

ACKNOWLEDGMENTS

This study was financially supported by the National Natural Science Foundation of China (Grant No. 42202206). We thank the lab member Zhiting Di for her assistance with lab equipment.

Conflicts of Interest

The authors declare that they have no known competing financial interests or personal relationships that could have appeared to influence the work reported in this paper.

Data Availability Stability

The data presented in this study are available upon request from the corresponding author.

REFERENCES CITED

Achi, O. K. (1994). "Growth and coal-solubilizing activity of *Penicillium simplicissimum* on coal-related aromatic compounds," *Bioresource Technology* 48(1), 53-57. DOI: 10.1016/0960-8524(94)90136-8

Akimbekov, N. S., Digel, I., Tastambek, K. T., Marat, A. K., Turaliyeva, M. A., and Kaiyrmanova, G. K. (2022). "Biotechnology of microorganisms from coal environments: From environmental remediation to energy production," *Biology* 11(9), article 1306. DOI: 10.3390/biology11091306

Barth, T., Høiland, S., Fotland, P., Askvik, K. M., Pedersen, B. S., and Borgund, A. E. (2004). "Acidic compounds in biodegraded petroleum," *Organic Geochemistry* 35(11–12), 1513-1525, DOI: 10.1016/j.orggeochem.2004.05.012.

Baylon, M. G., David, Y., Pamidimarri, S. D. V. N., Baritugo K. A., Chae C. G., Kim Y. J., Kim T. W., Kim M. S., Na J. G., and Park S. J. (2017). "Bio-solubilization of the untreated low rank coal by alkali-producing bacteria isolated from soil," *Korean Journal of Chemical Engineering* 34, 105-109. DOI: 10.1007/s11814-016-0252-x

Cohen, M. S., and Gabriele, P. D. (1982). "Degradation of coal by the fungi *Polyporus versicolor* and *Poria monticola*," *Applied and Environmental Microbiology* 44(1), 23-27. DOI: 10.1128/aem.44.1.23-27.1982.

Dahdouh, A., Bachir-Bey, M., and Kati, D. E. (2020). "Optimization of peroxidase activity of turnip (Brassica rapa) using response surface methodology," *Food Technology* (Series E) 24(2), 186-194. DOI: 10.2478/aucft-2020-0017

Elbeyli, İ. Y., Palantöken, A., Pişkin, S., Kuzu, H., and Peksel, A. (2006). "Liquefaction/solubilization of low-rank Turkish coals by white-rot fungus (*Phanerochaete chrysosporium*)," *Energy Sources, Part A: Recovery, Utilization, and Environmental Effects* 28(11), 1063-1073. DOI: 10.1080/00908310600626713

Fakoussa, R., and Hofrichter, M. (1999). "Biotechnology and microbiology of coal degradation," *Biotechnology and Microbiology of Coal Degradation* 52, 25-40. DOI: 10.1007/s002530051483

Feng, X. L., Sun, J. L., and Xie, Y. C. (2021). "Degradation of Shanxi lignite by *Trichoderma citrinoviride*," *Fuel* 291, article ID 120204. DOI: 10.1016/j.fuel.2021.120204

Galib, M. A., Abbott, T., and Lee, H. S. (2021). "Examination of extracellular polymer (EPS) extraction methods for anaerobic membrane bioreactor (AnMBR) biomass," *Sustainability* 13, article 12584. DOI: 10.3390/su132212584

Guo, H. Y., Zhou, D., Liu, X. L., Bai, Y., Gao, Z. X., and Xia, D. P. (2018). "Analysis of methanogens adsorption and biogas production characteristics from different coal surfaces," *Environmental Science and Pollution Research* 26, 13825-13832. DOI: 10.1007/s11356-018-3219-0

Hofrichter, M., and Fritsche, W. (1996). "Depolymerization of low-rank coal by extracellular fungal enzyme systems," *Applied Microbiology and Biotechnology* 46, 220-225. DOI: 10.1007/s002530050808

Huang, Z. X., Liers, C., Ullrich, R., Hofrichter, M., and Urynowicz, M. A. J. F. (2013). "Depolymerization and solubilization of chemically pretreated powder river basin subbituminous coal by manganese peroxidase (MnP) from *Bjerkandera adusta*," Fuel 112, 295-301. DOI: 10.1016/j.fuel.2013.04.081

Indriyani, D. M., Nurhasanah, N., and Herasari, D. (2021). "Optimization of lipase production from local bacteria isolate with palm oil inducer," *Jurnal Kimia Sains dan Aplikasi* 24(2), 58-61. DOI: 10.14710/jksa.24.2.58-61

Khan, M. T., Kaushik, A. C., Rana, Q. U. A., Malik, S. I., Khan, A. S., Wei, D. Q., Sajjad, W., Ahmad, S., Ali, S., Ameenullah, and Irfan, M. (2020). "Characterization and synthetic biology of lipase from *Bacillus amyloliquefaciens* strain," *Archives of Microbiology* 202(6), 1497-1506. DOI: 10.1007/s00203-020-01869-0

Li, B., Zhang, W., Xie, Z. H., Chen, X. J., and Cui, Y. (2024). "FTIR and XRD microscopic characterisation of coal samples with different degrees of

metamorphism," *Journal of Molecular Structure* 1309, article ID 138270. DOI: 10.1016/j.molstruc.2024.138270

Li, C. Y., Hu, W. C., Pan, B., Liu, Y., Yuan, S. F., Ding, Y. Y., Li, R., Shen, B., and Shen, Q. J. P. (2017). "Rhizobacterium *Bacillus amyloliquefaciens* strain sqrt3-mediated induced systemic resistance controls bacterial wilt of tomato," *Pedosphere* 27(6), 1135-1146. DOI: 10.1016/s1002-0160(17)60406-5

Li, Q. Z., Tao, Q. L., Yuan, C. C., Zheng, Y. N., Zhang, G. Y., Liu, J. F. (2018). "Investigation on the structure evolution of pre and post explosion of coal dust using X-ray diffraction," *International Journal of Heat and Mass Transfer* 120, 1162-1172. DOI: 10.1016/j.ijheatmasstransfer.2017.12.137

Machnikowska, H., Pawelec, K., and Podgórska, A. (2002). "Microbial degradation of low rank coals," *Fuel Processing Technology* (77–78), 17-23, DOI: 10.1016/S0378-3820(02)00064-4

Malik, A. Y., Ali, M., Jamal, A., and Ali, M. I. (2016). "Isolation and characterization of coal solubilizing aerobic microorganisms from Salt Range Coal Mines, Pakistan," *Geomicrobiology Journal* 34(2), 109-118. DOI: 10.1080/01490451.2016.1143538

Mei, J., Shen, X., Gang, L., Xu, H., Wu, F., and Li, S. (2020). "A novel lignin degradation bacteria – *Bacillus amyloliquefaciens* sl-7 used to degrade straw lignin efficiently," *Bioresource Technology* 310, article ID 123445. DOI: 10.1016/j.biortech.2020.123445

Nsa, I. Y., Akinyemi, B. T., Bello-Akinosho, M., Ezechukwu, S. N., Bayode, T. B., Igbinigie, E. E., and Adeleke, R. A (2022). "Development of a saprophytic fungal inoculum for the biodegradation of sub-bituminous coal," *Discover Applied Sciences* 4(2), article Number 53. DOI: 10.1007/s42452-021-04925-6

Pietrzak, R., Grzybek, T., and Wachowska, H. (2007). "XPS study of pyrite-free coals subjected to different oxidizing agents," *Fuel* 86, 2616-2624. DOI: 10.1016/j.fuel.2007.02.025

Ralph, J. P., and Catcheside, D. E. A. (1994). "Depolymerisation of macromolecules from Morwell brown coal by mesophilic and thermotolerant aerobic microorganisms," *Fuel Processing Technology* 40(2–3), 193-203, DOI: 10.1016/0378-3820(94)90142-2

Rasiya, K. T., and Denoj, S. (2021). "Iturin and surfactin from the endophyte *Bacillus amyloliquefaciens* strain rkea3 exhibits antagonism against staphylococcus aureus," *Biocatalysis and Agricultural Biotechnology* 36, article ID 102125. DOI: 10.1016/j.bcab.2021.102125

Rath, S., Paul, M., Behera, H. K., and Thatoi, H. (2022). "Response surface methodology mediated optimization of lignin peroxidase from *Bacillus mycoides* isolated from simlipal biosphere reserve, Odisha, India," *Journal of Genetic Engineering and Biotechnology* 20(1), article ID 2. DOI: 10.1186/s43141-021-00284-2

Rehman, M. Z. U., Akhtar, K., Khan, A. N., Tahir, M. A., Khaliq, S., Akhtar, N., and Ragauskas, A. J. (2022). "Bioconversion and quantification of humic substances from low rank coals using indigenous fungal isolates," *Journal of Cleaner Production* 376, article ID 134102. DOI: 10.1016/j.jclepro.2022.134102

Robbins, S. J., Evans, P. N., Esterle, J. S., Golding, S. D., and Tyson, G. W. (2016) "The effect of coal rank on biogenic methane potential and microbial composition," *International Journal of Coal Geology* 154–155, 205-212, DOI: 10.1016/j.coal.2016.01.001

Romanowska, I., Strzelecki, B., and Bielecki, S. (2015). "Biosolubilization of Polish brown coal by *Gordonia alkanivorans* S7 and *Bacillus mycoides* NS1020," *Fuel* Processing Technology 131, 430-436. DOI: 10.1016/j.fuproc.2014.12.019

Schmid, R. D., and Verger, R. (1998). "Lipases: Interfacial enzymes with attractive applications," *Angewandte Chemie International Edition in English* 37(12), 1608-1633. DOI: 10.1002/(SICI)1521-3773(19980703)37

Shi, C., Liu, X. R, Yang, Z. W., and Zhao, S. S. (2024). "Biodegradations of three different rank coals by a newly isolated bacterium *Bacillus* sp. Xk1," *Energy* 299, article ID 131441. DOI: 10.1016/j.energy.2024.131441

Shi, C., Liu, X. R., Zhao, S. S., and Yang, Z. W. (2023). "Additions of esterase and rhamnolipid promote the degradation of Inner Mongolia coal by *Pseudomonas japonica*," *Fuel* 340, article ID 127640. DOI: 10.1016/j.fuel.2023.127640

Shi, K. Y., Tao, X. X., Yin, S. D., Du, Y., and Lv, Z. P. (2009). "Bio-liquefaction of Fushun lignite: Characterization of newly isolated lignite liquefying fungus and liquefaction products," *Procedia Earth and Planetary Science* 1(1), 627-633. DOI: 10.1016/j.proeps.2009.09.099

Sivrikaya, O. (2014) "Cleaning study of a low-rank lignite with DMS, Reichert spiral and flotation," *Fuel* 119, 252-258. DOI: 10.1016/j.fuel.2013.11.061

Song, H., Liu, G., and Wu, J. (2016). "Pyrolysis characteristics and kinetics of low rank coals by distributed activation energy model," *Energy Conversion and Management* 126, 1037-1046. DOI: 10.1016/j.enconman.2016.08.082

Wu, H., Liu, X. R., Shi, C., Yang, J., Yang, Z. W., and Zhao, S. S. (2022). "Action modes of surfactants on biodegradation of Wudong low-rank coal by *Pseudomonas aeruginosa*," *Research Square*, Available Online. DOI: 10.21203/rs.3.rs-1410150/v1

Xia, W. C., and Zhang, W. (2017). "Characterization of surface properties of Inner Mongolia coal using FTIR and XPS," *Energy Source* 39(11), 1190-1194. DOI: 10.1080/15567036.2017.1315758

Xia, W. C., Xie, G. Y., and Peng, Y. L. (2015). "Recent advances in beneficiation for low rank coals," *Powder Technology* 277, 206-221. DOI: 10.1016/j.powtec.2015.03.003

Xiao, X., Zhang, Y. J., Wang, Z. G., Jin, D., Yin, G. S., and Liu, W. Q. (2009). "Characterization of coal oil using three-dimensional excitation and emission matrix fluorescence spectroscopy," *Chinese Optics Letters* 7(1), 85-87. DOI: 10.3788/col20090701.0085

Xu, C., Xin, T., Xu, G.., Li, X.., Liu, W., and Yang, Y. (2017). "Thermodynamic analysis of a novel solar-hybrid system for low-rank coal upgrading and power generation," *Energy* 141, 1737-1749. DOI: 10.1016/j.energy.2017.11.046

Yang, Y. L., and Feng, J. I. A. Q. (2022). "Study on difference of biogas production in different rank coal," *Coal Science and Technology* 50(10), 242-250. DOI: 10.13199/j.cnki.cst.MCQ20-044

Yao, J., Xiao, L., and Wang, L. (2012). "Separation and analysis of lignite bioconversion products," *International Journal of Mining Science and Technology* 22(4), 529-532. DOI: 10.1016/j.ijmst.2012.01.015

Yin, S. D., Tao, X. X., Shi, K. Y., and Tan, Z. C. (2009). "Biosolubilisation of Chinese lignite," *Energy* 34(6), 775-781. DOI: 10.1016/j.energy.2009.02.009

Zhang, N., Zhang, J. L., Wang, G. W., Ning, X. J., Meng, F. Y., Li, C. H., Ye, L., and Wang, C. (2022). "Physicochemical characteristics of three-phase products of low-rank coal by hydrothermal carbonization: Experimental research and quantum

chemical calculation," *Energy* 261, article ID 125347. DOI: 10.1016/j.energy.2022.125347

Zhou, J., Wang, J. J., Baudon, A., and Chow, A. T. (2013). "Improved fluorescence excitation-emission matrix regional integration to quantify spectra for fluorescent dissolved organic matter," *National Center for Biotechnology Information* 42(3), 925-930. DOI: 10.2134/jeq2012.0460

Article submitted: April 7, 2025; Peer review completed: June 7, 2025; Revised version received and accepted: July 1, 2025; Published: July 11, 2025.
DOI: 10.15376/biores.20.3.7211-7231